Digest Journal of Nanomaterials and Biostructures Vol. 14, No. 3, July - September 2019, p. 655 - 666

CONTROLLABLE SYNTHESIS AND GROWTH MECHANISM OF POROUS SnO_2 NANOSPHERES/GRAPHENE COMPOSITE

Y. W. YANG[a,*], L. Z. FANG[a], J. G. LIU[a], X. G. FANG[a], R. D. REN[a], Y. F. CHEN[a,b], Q. G.GAO[b], D. CHEN[c]

[a]*School of Materials Science and Engineering, Hefei University of Technology, Hefei, 230009, Anhui Province, P. R. China*

[b]*Anhui Aixian Magnet Device Technology Co., Ltd., Chuzhou, 239000, Anhui Province, P.R.China*

[c]*School of Instrument Science and Opto-electronics Engineering, Hefei University of Technology, Hefei, 230009, Anhui Province, P. R. China*

Graphene and its composites are expected to be the promising candidate for electrode materials of lithium-ion battery. However, the fabrication of graphene-based materials is a challenge and the related growth mechanism has not been clarified up to date. Here, the porous SnO_2 nanospheres/graphene composite is prepared by the *in situ* hydrothermal method. The article focuses on research and discussed the influence of preparation conditions, such as GO, HCl, temperature and time ect., on the morphology of the composites. This work reveals the growth mechanism of the porous SnO_2 nanospheres/graphene composite, which may contribute to the correct understanding of graphene-based materials for designing or fabricating the electrode materials of lithium-ion battery.

(Received March 4, 2019; Accepted August 9, 2019)

Keywords: Porous SnO_2 nanospheres, Graphene, Composite materials, Growth mechanism, Electrochemical properties

1. Introduction

As a kind of rechargeable battery, the main working principle of lithium-ion battery (LIB) is mainly to rely on the movement of lithium ions between the anode and cathode. Therefore, the discovery and development of new anode materials, such as nanostructure materials, metal oxide, graphene-based materials, has triggered a great interest to meet the ever-growing performance demands [1-3]. Among all those, tin oxide(SnO_2) nanomaterials has attracted considerable attention as potential substitutes for graphite because of high theoretical capacity, low cost, high surface-to-volume ratio, and widespread availability [4]. However, the poor conductivity and large volume expansion during lithium/sodium ion insertion/extraction process of SnO_2 are two important factors limiting its using in the anode electrode [5]. Taking into account the above two aspects, graphene with high mechanical strength and high electrical conductivity has been widely used to fabricate the SnO_2/grapheme composites and used as new type anode materials [6]. But,

*Corresponding author: hfutyyw@hfut.edu.cn

how to design and control the experimental parameters is still a challenge and needs to be addressed.

As a unique two-dimensional material, graphene has attracted a great deal of attention due to a series of singular features, such as high Young's modulus, high electromic stability and mechanical strength [7] in the past few years. It is desirable to harness the useful properties of graphene and its derivatives in composites through the incorporation with various kinds of functional materials [8]. In 2009, Honma's group [9] reassembled a 3D delaminated structure SnO_2/Graphene electrode for the first time, and its cycling performance is drastically enhanced in comparison with that of the bare SnO_2. After that, a number of effective strategy are proposed and developed to prepare SnO_2/graphene (SNG)composites with good electrochemical properties, such as the microwave-assisted method [10,11], hydrothermal Method [12], solvent-evaporation induced codeposition[13], template electrostatic spray deposition(ESD) [14], atomic layer deposition (ALD) [15], mechano-chemical ball milling (MBM)[16] and filtration method [17,18]. As a kind of wet chemical route, hydrothermal reaction method has got tremendous attention for synthesize of SnO2/graphene due to its low cost, high efficiency and environmentally friendly. The hydrothermal procedure is an efficient method for preparation of nanostructure material [19]. However, it is important to precise control of experimental parameter like time, temperature, content and pH of precursor solution etc. for the production of different nanostructures. Chen et al. showed that the annealing treatment contributes to the formation of the Sn-O-C bonds between the SnO_2 nanoparticles and the reduced graphene sheets [20]. It is believed that the design of synthesized route and precise control of experiment conditions are essential [21]. S. Ramaprabhu et al. think that the hydrothermal route is a multistep, long time consuming process of glycol reduction, hydrothermal and thermal treatment [22]. Based on these results, it is meaningful to design and research experimental parameters of hydrothermal reaction to improve the electrochemical performance of SnO_2/G.

In order to develop an anode material with high capacity and cyclic stability, we have reported the preparation of the porous hollow SnO_2 nanosphere and porous SnO_2 nanospheres/graphene composite in the past two years [23,24]. In this work, the emphasis is to study the influence of preparation conditions on the structure and morphology of the porous SnO_2 nanospheres/graphene composites (pSNG) and to explore their forming mechanism by the method of *in situ* hydrothermal.

2. Experimental

2.1. Materials

All the chemicals reagents in the experiments were used without further purification. Graphite flake (325 mesh) were purchased from Qingdao Jinri Graphite Co., Ltd, China. Sodium dodecyl sulfate (SDS, AR), Tetraethylorthosilicate (TEOS, AR) and NaOH (AR) were obtained from Sinopharm Chemical Reagent Co. Ltd., China.

2.2. Synthesis of sample

Graphene oxide (GO) sheets were synthesized from natural graphite powder by the modified Hummers' method[25], and used as the precursor. The SnO2 nanospheres /graphene

(SnO_2/G) composite were prepared by a simple hydrothermal route. Specifically, GO (25mg) was added into distilled water (0.3ml) with ethanol (30ml) respectively, sodium dodecyl sulfate (SDS) (280mg) was then added, followed by 1 h ultra-sonication to make a homogeneous suspension. Then, $SnCl_2$-$2H_2O$ (250mg) and concentrated HCl were added into the suspension respectively. After 5 minutes of ultrasonic treatment, the mixture was dissolved in the mixture under magnetic stirring at room temperature for minutes. Finally, the resulting solution was transferred to 50 ml Teflon-lined stainless steel autoclave for the hydrothermal syntheses at 180℃ for 12h in an electrical oven. After heating treatment, the autoclave was cooled to room temperature. Black products were obtained by centrifugation, washed with distilled water several times prior to be dried in vacuum at 60℃. In order to explore the effects of different hydrothermal reaction conditions on the product, we changed the amount of the GO (15mg, 25mg, 35mg) and HCl (0.3ml, 0.6ml, 0.8ml, 1ml) the temperature(160℃, 180℃, 200℃) and time(12 h, 16h, 24h) of hydrothermal reaction, respectively. The resultant composites were obtained, in which the sample was denoted as the S_x(x=1,2…10) . The samples and experimental parameters are listed in Table 1.

Table 1. the BET specific surface area of pSNG with different P/P_0.

P/P_0	*0.0807*	*0.103*	*0.152*	*0.201*	*0.250*	*0.299*	*0.348*	*0.397*
V/(cm^3g^{-1})	16.558	16.619	18.430	20.183	21.920	23.666	25.460	27.299
S/ (m^2 g^{-1})	73.053	70.148	70.808	71.710	72.621	73.341	73.834	74.116

2.3. Sample characterization

The structure and morphology of the samples were investigated by transmission electron microscopy(HRTEM,JEOLJEM-2100F), scanning electron microscopy (FESEM, HITACHISU8020). The Crystal structures of products were characterized by X-ray diffraction (XRD,RigakuD/MAX-RC) with Cu Kα radiation (λ=1.518Å). The functional groups in samples were characterized by Fourier transform infrared spectrometry (FT-IR, Nicolet 67, USA Thermo Nicolet). The composition analysis in samples were performed by X-ray photoelectron spectroscopy (XPS, ESCALAB250, USA Thermo) in the region of 0-1400 eV. Furthermore, the N_2 adsorption/desorption measurements at 77 K were further examined to determine the porous structure of the materials.

2.4. Electrochemical measurements

Electrochemical properties of the as-prepared materials were evaluated with CR2032-type coin cells. To prepare working electrodes, the samples were mixed with acetylene black and polyvinylidene fluoride (PVDF) in a weight ratio of 7:2:1in N-methylpyrrolidinone (NMP) solvent. Then, the slurry was uniformly cast on a copper foil and dried at 90°C in vacuum for 12h. The coin cells were assembled inside an argon-filled glovebox using lithium metal foil as the counter electrode and the polypropylene as the separator. The electrolyte was 1M $LiPF_6$ dissolved in ethylene carbonate (EC) and dimethyl carbonate (DMC) solvent (1:1 volume ratio). A galvanostatic cycling test of the assembled cells was carried out on a Land CT2001A system in the potential range of 0.05-2.00V (vs Li^+/Li) at a discharge/charge current density of 400 $mA \cdot g^{-1}$.

3. Results and discussion

3.1 Morphology and structure characterization

In this experiment, the effects of experimental parameters, such as amount of the GO, HCl, hydrothermal temperature and time, on the pSNG were studied. Fig. 1 is the TEM images of the pSNG composites obtained from different amount of the GO(S1,S2,S3). As we can see, with the increase of the amount of the GO, the diameter of the SnO_2 nanospheres become larger. At the same time, along with the increase of the content of GO, SnO_2 nanosphere morphology has changed. The fig.1 confirms that the content of GO has a direct impact on the size and morphology of SnO_2 nanosphere and the shape of sample S2 relatively is regular, most present a spherical edges structure (Fig.1 b).

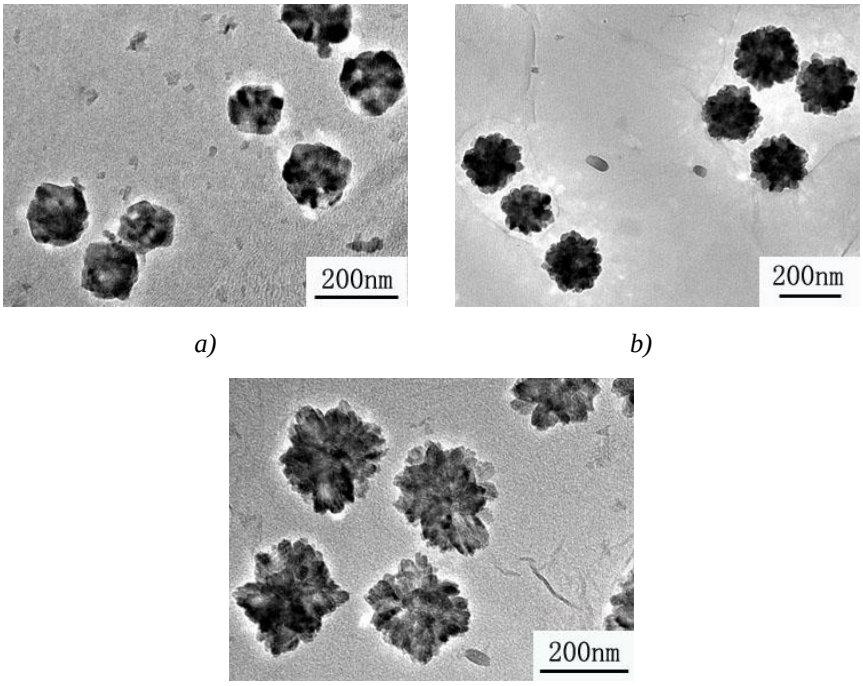

a) *b)*

c)

Fig. 1. TEM images for S1, S2 and S3.

In this synthesis method, adding suitable amount of hydrochloric acid plays a critical role in obtaining porous hollow SnO_2 nanospheres (Fig. 2). It can be seen clearly from the Fig. 2 (a) that when the HCl content in the precursor solution is too low (0.3 ml), the nanoparticles or even amorphous structures which consist of more abundant weeny nanoparticles are obtained and some SnO_2 nanoparticles are stacked together on the graphene. With the increase of the count of HCl, the SnO_2 nanoparticles tend to accumulate to form the spheres structure. When HCl content increased to 1 ml, the average diameter of porous SnO_2 can reach about 285nm. The results showed that the acidic environment is beneficial to the nucleation and growth of SnO_2 nanosphere.

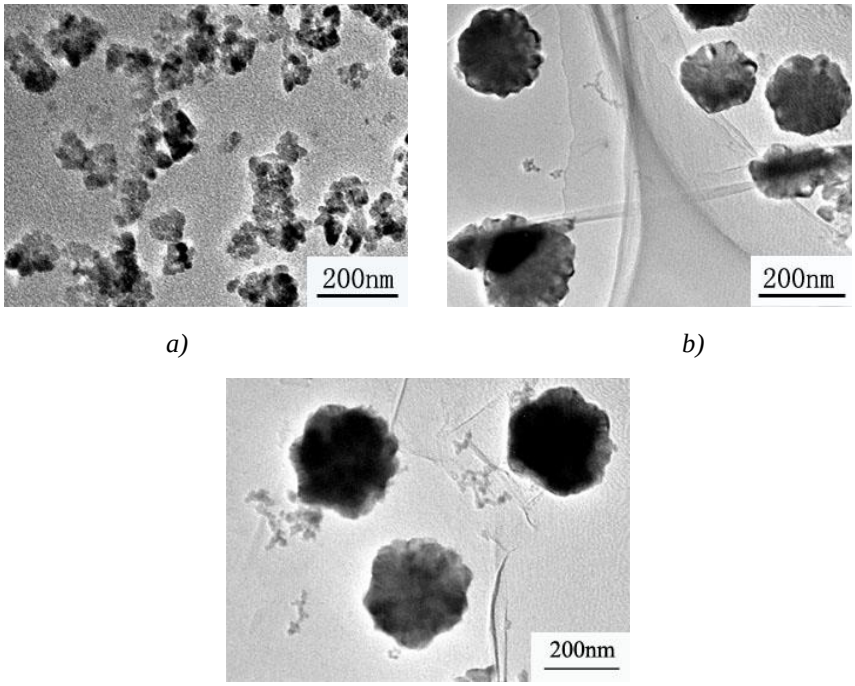

a) *b)*

c)

Fig. 2. TEM images for S4, S5 and S6.

Apart from the content of GO and HCl, the effect of hydrothermal reaction temperature and time are also investigated. As shown in the Fig. 3 (a, b), with the increase of reaction temperature, the diameter of the SnO_2 nanospheres is decreased compared with the S5. The hydrothermal reaction temperature directly affects the average size of nanospheres and the hollow degree of samples. At low temperature (160 ^{o}C), the as-prepared sample consists of many nearly solid nanospheres and the average diameter is more than 200 nm (Fig.2(b)). The size of the nanospheres at higher hydrothermal temperature (180 ^{o}C) reduce to 150 nm and the hollow structure is more pronounced (Fig. 3 (a)). When the reaction temperature rises to 220 ^{o}C, many smaller porous hollow nanospheres with an average diameter of 100nm are obtained (Fig.3(b)). According to the results, the water thermal response time directly affects the dispersion of SnO_2 nanospheres on the graphene sheet. We can see from the fig.3(c,d), whether it is 16 hours or 24 hours, the diameter of the nanometer ball did not significantly increased. But as time goes on, the nanospheres are more irregular in shape ,and the reunion is more and more serious.

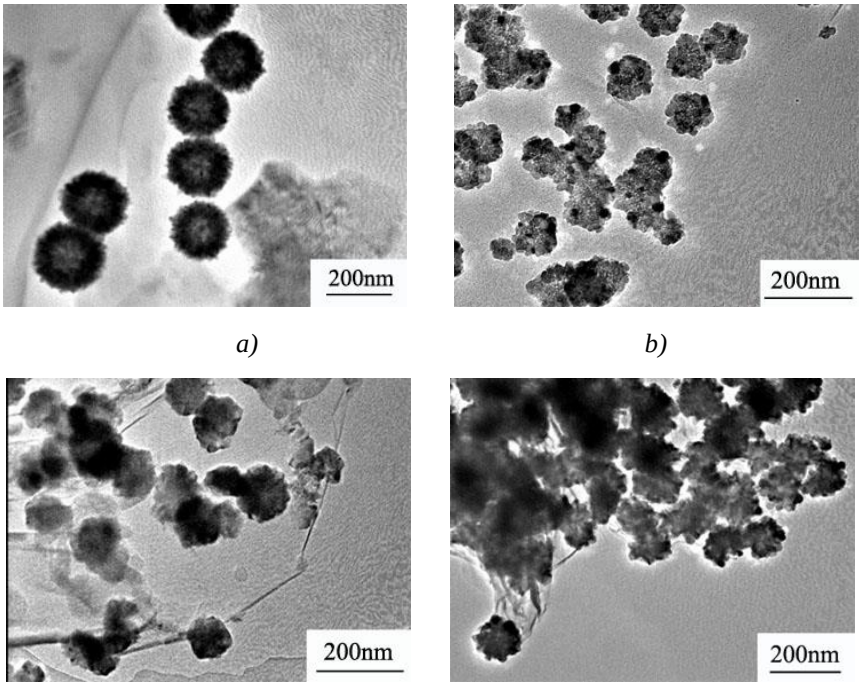

a) *b)*

c) *d)*

Fig. 3. TEM images for S7, S8,S9 and S10.

The FESEM image further indicates that the SnO_2 nanospheres have the smaller particles with diameters of 150–400nm, and disordered space exists among the smaller particles. Noticeable, Fig. 4 reveals that a lot of uniform SnO_2 nanospheres have been deposited onto the high quality graphene substrate regardless of the different reaction parameters. The resulting products (S2,S5,S7,S9) show that the SnO_2 nanospheres are homogeneously anchored onto the surface of two dimensional graphene sheets to format of pSNG. And we can see that the SnO_2 nanospheres with a diameter of 150-400nm have homogeneous morphology and porous structure. However, it could be clearly seen that SnO_2 nanospheres are not smooth(fig.4(c,d)), they are composed of many small SnO_2 nanocrystals. We think that the crystals radically ordered outwards, and get together to form the porous structure similar with durian-shaped which is in agreement with the TEM analysis.

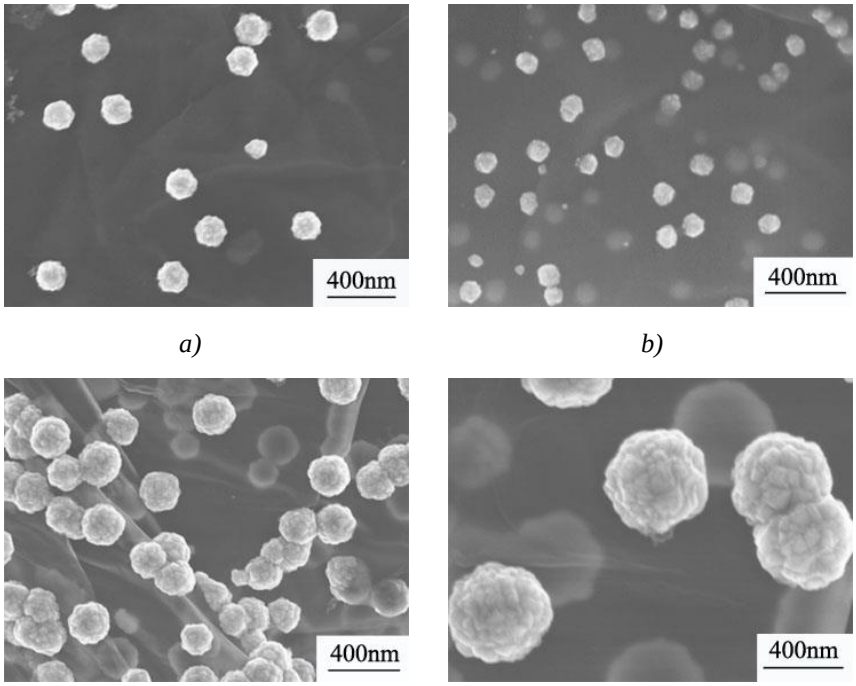

a) *b)*

c) *d)*

Fig. 4. The FE-SEM images of the pSNG composites(a:S2,b:S5,c:S7,d:S9).

The crystal structure of pSNG nanocomposites is investigated by XRD technique. As is illustrated in all curves, the three dominant broadened peaks (110), (101), and (211) are attributed to the SnO_2 phase (JCPDS No. 41-1445), indicating the formation of tetragonal SnO_2 nanocrystals with cassiterite structure. It can be seen from the diagram, SnO_2 nanometer ball can be obtained under different conditions and no other impurity peaks were observed. As we can see from the Fig. 5, no diffraction peaks of layered GO ($2\theta = 10.3°$) can be observed, indicates that the SnO_2 nanoparticles effectively inhibit the re-stacking of graphene nanosheets, in other words, that limits constructive diffractions from ordered graphene sheets, indirectly conforming the formation of pSNG nanocomposites [25]. Furthermore, the high intensity and sharp diffraction peaks of pSNG demonstrate that the size of SnO_2 is relatively larger.

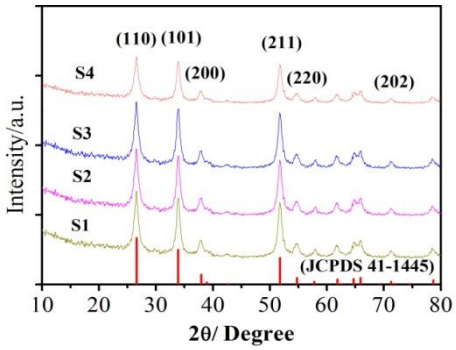

Fig. 5. XRD pattern of pSNG.

The N2 adsorption properties of pSNG were investigated to determine the porous structure of the composites. As is shown in Fig. 6, the pSNG exhibited N2 adsorption-desorption isotherms of Type Ⅳ with Type H2 hysteresis at high relative pressure [26]. The desorption isotherm differed from adsorption isotherm in the relative pressure 0.7 to 0.97, showing mesopores in the composites [27]. We can see that adsorption quantity increases gently in the low pressure stage (P/P0≤0.6) and the adsorption isotherms is same to the desorption isotherms. It can be seen from the Barretl—Joyner—Halenda(BJH) pore size distribution analysis(inset of fig.6) that the average pore size and pore volume of pSNG is 3.188 nm and 0.086 $cm^3 \cdot g^{-1}$ respectively. According to the experience relational table of P/P0 and S/V [28], we calculated the Brunauer-Emmett-Teller (BET) specific surface area of the pSNG at the different point (0.05< P/P0<0.40). As is shown in Table 2, the average BET specific surface area of pSNG was estimated to be **7**2.454 $m^2 \cdot g$-1. This is higher than that of SnO_2 nanoparticles, suggesting that the addition of graphene provides a larger specific surface area for the material, which could increase the contact area between electrode and electrolyte [29].

Table 2. The samples and experimental parameters.

No.	GO（mg）	HCl (ml)	Temperature (^{o}C)	Time (h)
S1	15	0.6	160	12
S2	25	0.6	160	12
S3	35	0.6	160	12
S4	25	0.3	160	12
S5	25	0.8	160	12
S6	25	1	160	12
S7	25	0.8	180	12
S8	25	0.8	200	12
S9	25	0.8	180	16
S10	25	0.8	180	24

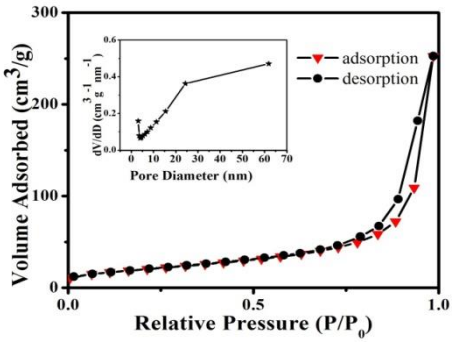

Fig. 6. N_2 adsorptione-desorption isotherms of pSNG.

3.2. Growth mechanism

Graphene has excellent thermal properties, optical properties, mechanical properties, and electrical properties, and shows great potential and value both in theoretical research and practical applications. Howerer, because of its unique geometric features and the interfacial instability, graphene is still quite difficult to directly apply as structure materials. Using graphene as constituent phase in composites thus has been considered as a versatile method to make use of

the excellent structural characteristics and physical properties of graphene [30]. As is shown in figure 7, pSNG composites with different SnO_2 contents were fabricated by *in situ* hydrothermal process using $SnCl_2$-$2H_2O$ as Sn precursors and distilled water as solvent. Briefly, the formation of pSNG composites can be described as two main steps: firstly, GO nanosheets with abundant functional groups are prepared through the modified Hummers method. Secondly, Sn^{2+} ions are hydrolyzed to SnO_2 nanosphere and then attach onto the surface of graphene sheets, in which the GO nanosheets were reduced to rGO. As is illustrated in Fig.7, natural flake graphite is oxidized by the Hummers method, the distance between the layers of graphite is increased greatly due to the formation of functional groups (e.g. hydroxyl, carboxyl, carbonyl and other groups). During the hydrothermal process, the reduced graphene oxide (rGO) was facilely prepared and the ethanol was introduced into the hydrothermal system to improve the reduction. At the same time, the primary SnO_2 nanoparticles further agglomerate to form dense nanospheres to reduce the overall Gibbs free energy. The oxygen functional groups were effectively removed by the reduction in the hydrothermal process, and the π-conjugated frame-work of graphene was effectively recovered. The reactions taking place in the Sn^{2+} and HCl mixed solution can be described as follows:

$$SnCl_2 + H_2O \rightarrow S_n(OH)Cl + HCl$$

$$Sn^{2+} + xCl^- \rightarrow S_nCl_x^{2-x}(x = 1,2,3or4)$$

Thus, how to improve the poor dispersibility and weak adhesion of graphene in the matrix of a composite material has become a vital problem[31]. In our experiment, HCl has a great influence on the growth process of the SnO_2 nanocrystals. When the content of concentrated HCl is too low, hydrolysis rate of Sn^{2+} is large and it is difficult to adsorption with Cl-. As is shown in Fig. 2 (a), small SnO_2 nanoparticles are difficult to grow into nanospheres with a large diameter [32]. It means that addition of concentrated HCl can further inhibit the hydrolysis of Sn^{2+} ions. On the contrary, along with the content of HCl increasing, the hydrolysis rate of Sn^{2+} is falling. As a result, the generated SnO_2 nanoparticles have enough time to reunite together, get a spherical SnO_2 particles after curing. These porous spherical SnO_2 nanoparticles dispersed on the surface of graphene, forms a "sandwich" structure of porous SnO_2 nano ball/graphene nano composite structure. FESEM observation (Fig. 4) clearly confirmed the successful deposition of the SnO_2 nanoparticles on graphene nanosheets. Because graphene is made of graphite oxide reduction, so there will be many remaining valence, the surface functional groups, epoxy compound, SnO_2 nanometer ball formation and key bridge, generate strong interface binding force, which can make the SnO_2 nanometer ball firmly attached on the surface of graphene.

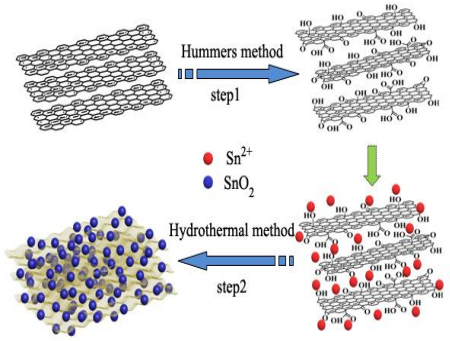

Fig. 7. Schematic formation process of the pSNG composites.

3.3. Electrochemical properties

To investigate the electrochemical performance, the pSNG (S7) is discharged and charged at a rate of 400 mA·g^{-1}. The capacity profiles of the same cell at various cycles for the 1st, 2nd, 10th and 50th are illustrated in Fig. 6. In the first cycle, the Sn/graphene electrode delivered a discharge capacity of 2001 mAh·g-1 and a reversible charging capacity of 952.2 mAh·g-1. The irreversible capacity could be mainly ascribed to the formation of the Sn, Li_2O and solid electrolyte interphase (SEI) layers on the surface of the electrode [33]. From the second cycle, the reversibility of the electrode was gradually improved on cycling. The electrode maintained a capacity of 658 mAh·g-1 after 50 cycles with an average columbic efficiency of 96.3% (586/683). The superior cycling performance is mainly due to the Special "sandwich" structure, which is made up of SnO_2 nanospheres and graphene matrix. It can be seen from Fig. 8 that the SnO_2 nanospheres serves as a spacer that keeps the neighboring graphene separated, hindered the reunion of graphene sheets. Due to its electronic property, the graphene layers could facilitate the formation of conductive networks, improve the conductivity and shorten the electronic transport route for Li-ions. Furthmore, the graphene could effectively prevent the volume expansion/contraction and aggregation of SnO_2 nanoparticles during Li ions charge/discharge process.

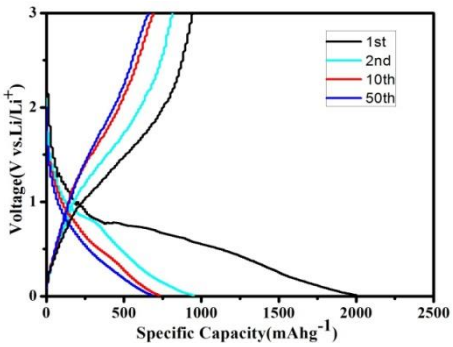

Fig. 8. The charge-discharge curves of the pSNG composites.

4. Conclusions

In summary, pSNG composites were fabricated by the *in situ* hydrothermal method and the influence of preparation conditions on the structure characteristic of the pSNG was discussed in detail. The morphological study of pSNG composites via TEM illustrated the influence of preparation conditions on the structure and morphology of the composites. The obtained information was again validated via SEM, XRD, absorption spectra. It is found that the amount of the GO, hydrochloric acid, reaction temperature and growth time are crucial factors in controlling the structure of the pSNG composites. Appropriate acidic solution is beneficial to the improvement of adhesion between the SnO_2 and rGO.

The diameter of the SnO_2 nanospheres increased with the increasing of the amount of GO, hydrothermal temperature and time. The enhancement of electrochemical performance is attributed to its porous sandwich structure, high specific surface area and enhanced conductivity. We hope that this study will inspire more specific research to explore the growth mechanism and controllable synthesis of graphene-metal oxide composites.

Acknowledgements

This work is financially supported by the Key Research and Development Project of Anhui Province (1804a09020063).

References

[1] R. Saroha, A.K. Panwar, A.R. Farooq, L. Krishniya, P.K. Tyagi, Ionics **23**, 2641 (2017).
[2] J.J. Wang, L.Y. Wang, S.Y. Zhang, S.Y. Liang, X.Q. Liang, H. Huang, W. Z. Zhou, J. Guo, J. Alloys Compd. **748**, 1013 (2018).
[3] M. Sahoo, S. Ramaprabhu, Carbon **127**, 627 (2018).
[4] M.K. Singh, R.K. Pandey, R. Prakash, Org. Electron. **50**, 359 (2018).
[5] H.G. Wang, C. Jiang, C.P. Yuan, Q. Wu, Q. Li, Q. Duan, Chem. Eng. J.**332**, 237 (2018).
[6] C.L. Zhu, Z.X. Chen, S.M. Zhu, Y.Li, H. Pan, X. Meng, M. Imtiaz, D. Zhang, Sci. Rep-UK. **7**(1), 3276 (2017).
[7] Y. F. Kao, C.I. Hung, S.H. Chang, J.W. Yeh, W.K. Hsu, Cryst. Eng. Comm.**16**, 6187 (2014).
[8] X. Huang, X. Y. Qi, F. Boey, H. Zhang, Chem. Soc. Rev. **41**, 666 (2012).
[9] S. M. Paek, E. J. Yoo, I. Honma, Nano Lett. **9**(1), 72 (2009).
[10] B. Dursun, E. Topac, R. Alibeyli, A. Ata, O. Ozturk, D.C. Rezan, J. Alloys Compd. **728**, 1305 (2017).
[11] A. Birrozzi, R. Raccichini, F. Nobili, M. Marinaro, R. Tossici, R. Marassi, Electrochim. Acta. **137**, 228 (2014).
[12] X.F. Chu, X.H. Zhu, Y.P. Dong, W.B. Zhang, L.S. Bai, J. Mater. Sci. & Technol. **31**, 913 (2015).
[13] L. Chen, X.H. Ma, M.Z. Wang, C.H. Chen, X.W. Ge, Electrochem. Acta. **215**, 42 (2016).
[14] Y. Z. Jiang, T. Z. Yuan, W. P. Sun, M. Yan, ACS Appl. Mater. & Interfaces **4**, 6216(2012).
[15] X. F. Li, X. B. Meng, J. Liu, D. S. Geng, Y. Zhang, Adv. Funct. Mater. **22**,1647 (2012).
[16] F. Ye, B. Zhao, R. Ran, Z. P. Shao, Chem. Eur. J. **20**, 4055 (2014).
[17] J. F. Liang, Y. Zhao, L. Guo, L. D. Li, ACS Appl. Mater. & Interfaces, **4**, 5742 (2012).
[18] T. Gao, K. Huang, X. Qi, H. X. Li, L. W. Yang, J. X. Zhong, Ceram. Int. **40**, 6891 (2014).
[19] M. Shojaee, S. Nasresfahani, M. H. Sheikhi, Sensor. & Actuat. B-Chem. **254**, 457 (2018).
[20] R. Tian, Y. Y. Zhang, Z. H, Chen, H. N. Duan, B. Y. Xu, Y. P. Guo, H. M. Kang, H. Li, H. Z. Liu, Sci. Rep-UK. **6**, 19195 (2016).
[21] W. B. Yue, S. Yang, Y. Ren, X. J. Yang, Electrochem. Acta **92**, 412 (2013).

[22] Y. Lei, X. Bing, Z. Zhang, C. Y. Fang, J. Mater. Sci. **28**, 17058 (2017).
[23] Y. W. Yang, D. M. Ma, T. Cheng, Y. H. Gao, Nano **10**(6), 15500873 (2017).
[24] Y. W. Yang, Y. H. Gao, T. Cheng, D. M. Ma, J. G. Liu, X. L. Li, RSC Adv. **6**, 67011 (2016).
[26] H. Q. Du, J. F. Bai, C. Y. Zuo, Z. F. Xin, J. B .Hu, Cryst. Eng. Comm. **13**, 3314 (2013).
[27] Y. Masuda, K. Kato, J. Cryst. **311**, 593 (2009).
[28] Z. G. Zhao, Application principle of adsorption, Chemical industry press, Beijing **1**, Ch. 6, p. 498 (2005).
[29] M. Y. Wang, Y. Huang, X. F. Chen, K. Wang, H. W. Wu, N. Zhang, H. T. Fu, J. Alloys Compd. **691**, 407 (2017).
[30] R. M. Gao, H. J. Zhang, S. Yuan, L. Y. Shi, M. G. Wu, Z. Jiao, RSC Adv. **6**, 4116 (2016).
[31] A.Y. Liang, X.S. Jiang, X. Hong, Y.X. Jiang, Z.Y. Shao, D.G. Zhu, Coatings **8**, 33 (2018).
[32] M. Ocana, E. Matijevic, J. Mater. Res. **5**, 1083 (1990).
[33] B. Anothumakkoola, N. Dupréa, P. Moreaua, D. Guyomarda, T. Broussea, J. Gaubichera, J. Power Sources **378**, 628 (2018).
[34] X.Y. Zhou, J.J. Shi, Y. Liu, Q.M. Su, J. Zhang, G.H. Du, J. Alloys Compd. **615**, 390 (2016).